AGU PUBLICATIONS

Water Resources Research

RESEARCH ARTICLE
10.1002/2014WR016228

Key Points:
- Integrated mathematical description of flow and temperature dynamics
- Spatially explicit simulations of streamflow and stream temperature
- Reliable prediction of seasonal hydrothermal cycles in Alpine catchments

Correspondence to:
F. Comola,
francesco.comola@epfl.ch

Citation:
Comola, F., B. Schaefli, A. Rinaldo, and M. Lehning (2015), Thermodynamics in the hydrologic response: Travel time formulation and application to Alpine catchments, *Water Resour. Res.*, *51*, 1671–1687, doi:10.1002/2014WR016228.

Received 31 JUL 2014
Accepted 9 FEB 2015
Accepted article online 13 FEB 2015
Published online 23 MAR 2015

Thermodynamics in the hydrologic response: Travel time formulation and application to Alpine catchments

F. Comola[1], B. Schaefli[2], A. Rinaldo[2,3], and M. Lehning[1,4]

[1]CRYOS Lab, École Polytechnique Fédérale de Lausanne, Lausanne, Switzerland, [2]ECHO Lab., École Polytechnique Fédérale de Lausanne, Lausanne, Switzerland, [3]Dept. of Civil, Environmental and Architectural Engineering, University of Padova, Padova, Italy, [4]WSL Institute for snow and Avalanche Research SLF, Davos, Switzerland

Abstract This paper presents a spatially explicit model for hydrothermal response simulations of Alpine catchments, accounting for advective and nonadvective energy fluxes in stream networks characterized by arbitrary degrees of geomorphological complexity. The relevance of the work stems from the increasing scientific interest concerning the impacts of the warming climate on water resources management and temperature-controlled ecological processes. The description of the advective energy fluxes is cast in a travel time formulation of water and energy transport, resulting in a closed form solution for water temperature evolution in the soil compartment. The application to Alpine catchments hinges on the boundary conditions provided by the fully distributed and physically based snow model Alpine3D. The performance of the simulations is illustrated by comparing modeled and measured hydrographs and thermographs at the outlet of the Dischma catchment (45 km^2) in the Swiss Alps. The Monte Carlo calibration shows that the model is robust and that a simultaneous fitting of streamflow and stream temperature reduces the uncertainty in the hydrological parameters estimation. The calibrated model also provides a good fit to the measurements in the validation period, suggesting that it could be employed for predictive applications, both for hydrological and ecological purposes. The temperature of the subsurface flow, as described by the proposed travel time formulation, proves warmer than the stream temperature during winter and colder during summer. Finally, the spatially explicit results of the model during snowmelt show a notable hydrothermal spatial variability in the river network, owing to the small spatial correlation of infiltration and meteorological forcings in Alpine regions.

1. Introduction

In Alpine catchments, a significant amount of precipitation is stored as snow and ice throughout an extended period of time before the start of the melting process at the beginning of the summer season. Accordingly, snow and ice are very important water resources not only for mountain catchments but also for large and dry lowland areas of western America, central Asia, northern India, and southern Europe [*Barnett et al.*, 2005; *Trujillo and Molotch*, 2014]. This yearly accumulation and melt of snow and ice give rise to strong annual hydrological cycles, with pronounced low flows during the winter [*Schaefli et al.*, 2013], melt-driven high flows throughout the summer, and strong recessions during fall [*Biswal and Marani*, 2010; *Mutzner et al.*, 2013]. Given that the yearly cycle of snow accumulation and melt strongly depends on temperature, the global warming widely predicted by climate models will most likely have a strong impact and the hydrologic regime of Alpine catchments. Recent investigations suggest that a shift in the streamflow peak from summer to spring may be expected due to the warming-induced earlier melting of snow and ice [e.g., *Bavay et al.*, 2009, 2013], possibly accompanied by lower glacier melt rates [*Stahl et al.*, 2008] and a change in snow cover [*Stewart et al.*, 2005].

The hydrologic regime of Alpine catchments has a strong impact on their thermal response [*Brown and Hannah*, 2007] due to the different temperatures of the streamflow sources, i.e., meltwater from glaciers and snowpack [*Finger et al.*, 2013], karstic groundwater, and hillslope aquifers [*Brown et al.*, 2005]. The thermal regime of Alpine catchments, in turn, strongly controls ecological processes, as many freshwater organisms tend to migrate according to their temperature preferences [*Coutant*, 1977]. The thermal cycle of Alpine streams generally presents a close to freezing temperature during winter, an increasing phase from spring to summer and a descending phase in autumn. In recent years, the scientific community has developed a great interest in the effects of climate change on stream temperature [*Matulla et al.*, 2007; *Kurylyk et al.*, 2013].

A intensive analysis of high-resolution records collected by *Hari et al*. [2006] in 25 Alpine streams in Switzerland demonstrated that significant warming has taken place during the last 25 years of the 20th century. The stream network being an important ecological corridor [*Ward and Tockner*, 2001], the warming climate is thus expected to cause a redistribution, if not even the extinction, of many aquatic species [*Mohseni et al*., 2003].

All these investigations emphasize the strong interconnection between streamflow, stream temperature, and ecosystem services, suggesting that a reliable model for flow and temperature simulations in Alpine streams may be an extremely useful tool to predict the impacts of climate, land use, or water management changes on water resources and biodiversity. Numerical simulations are, however, a challenging task, due to the complexity and space-time variability of meteorology, near-surface snow processes, transport, and exchange dynamics in soils and channel networks. The existing modeling approaches differ from each other in terms of spatial detail, ranging from fully distributed to lumped models, and physical representativeness, ranging from physically based to conceptual models. For a review of rainfall-runoff and stream temperature models, see e.g., *Todini* [2007] and *Caissie* [2006], respectively.

The physical description of the transport dynamics may be addressed through a Lagrangian or an Eulerian framework that formally differ from each other but both are derived from conservation equations in a control volume. The formulation of transport by travel time distribution arises in a Lagrangian stochastic context and has initially been applied to provide a statistical mechanical description of solute mass response functions [*Rinaldo and Marani*, 1987; *Rinaldo et al*., 1989] and geomorphological dispersion in the hydrologic response [*Rinaldo et al*., 2006, 1991; *Rinaldo and Rodriguez-Iturbe*, 1996]. More recently, the travel time framework has led to theoretical advances in the description of soil moisture dynamics [*Botter et al*., 2010; *Rinaldo et al*., 2011] and kinematics of water age mixing in soils [*Benettin et al*., 2013a]. On the modeling side, successful applications of the travel time formulation of reactive solutes transport [*Botter et al*., 2005] have been achieved by *Bertuzzo et al*. [2013] and *Benettin et al*. [2013b].

In this study, we seek a novel approach to simulate hydrologic and thermal regimes, describing the mass and energy transport in soil compartments with a travel time framework. The application of the derived formulation to Alpine catchments relies on the boundary conditions provided by Alpine3D, the physically based and fully distributed model of snow processes developed at the WSL institute for snow and avalanche research [*Lehning et al*., 2006]. The theoretical relevance of the work stems from an extension of previous travel time frameworks to a more complete treatment that includes the energy dynamics. From a practical prospective, we believe that the coupled and spatially explicit simulation of streamflow and temperature is promising for future investigations of ecohydrological processes in Alpine regions.

In section 2, we derive the travel time formulation of energy transport at subcatchment scale, recalling previous results on the age mixing theory [*Botter et al*., 2010]. In fact, the age of water cannot be disregarded when simulating the concentration in water of reactive scalars, such as chemicals or temperature, for which the exchange processes strongly depend on the contact time between mobile (water) and immobile (soil) phases. In section 3, the numerical model used to solve the coupled hydrothermal problem is introduced. Following, the case study of the high Alpine Dischma catchment (Grisons, Switzerland) is described. The numerical results are discussed in section 5 and conclusions finally close the paper.

2. Theoretical Framework

In this section, we propose a travel time formulation of mass and energy transport at subcatchment scale, resulting in a closed form solution of water temperature evolution in the soil compartment. In order to facilitate the reading, we also provide a list of the recurrent symbols in the notation section.

2.1. Mass Transport

The travel time formulation of water transport that we present hereafter was initially proposed by *Botter et al*. [2010], who derived and discussed the equations in much details. In this section, we provide a concise and effective recall of those results that are essential to further derive the formulation of energy transport.

Let us assume the control volume to be the portion of soil delimited, laterally, by the water divide of the catchment and bounded by the land surface. The lower boundary is considered as a deep and impervious surface [e.g., *Brutsaert*, 2005]. The domain can be further decomposed in smaller units, called subcatchments, each of them defined as the portion of a catchment draining into a single stream of the river

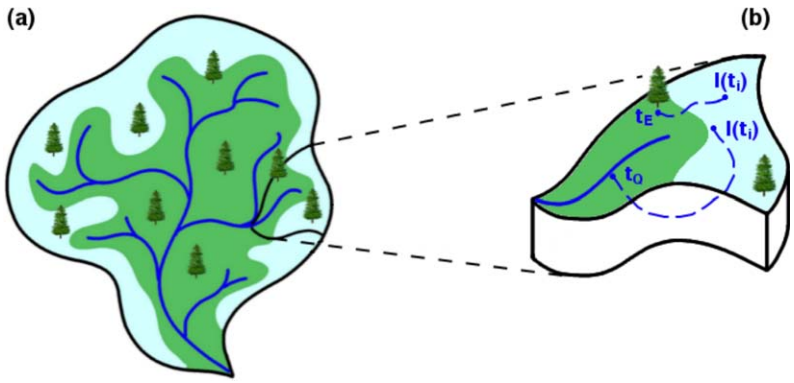

Figure 1. (a) Subdivision of the catchment into source areas (subcatchments) assumed to be independent hydrological control volumes. Each subcatchment drains water into a single stream, which can be of order 1 or higher. (b) Trajectory of generic transport volumes, infiltrating at injection time t_i and leaving the control volume through evapotranspiration, after a travel time t_E, or through subsurface flow, after a travel time t_Q.

network, as shown in Figure 1a. The subcatchment water storage $S(t)$ (m) is fed by the infiltration $I(t)$ (m s^{-1}) occurring at the land surface and depleted by subsurface flow into the stream $Q(t)$ (m s^{-1}) and evapotranspiration $E(t)$ (ms^{-1}). All the introduced variables are expressed per unit subcatchment area.

Let $I(t_i)dt_i$ (m) be a transport volume infiltrating at the injection time t_i and $t-t_i$ (s) be its travel time, i.e., the time elapsed between t_i and the time $t > t_i$ at which the transport volume leaves the subcatchment through $Q(t)$ or $E(t)$. The travel time is, in general, a function of the injection time, as it strongly depends on the moisture content of the soil at the time at which the particle infiltrates [*Rinaldo et al.*, 2011]. Every transport volume injected in the subcatchment at time t_i follows a different trajectory and presents a different value of travel time. One may thus consider the travel time of each transport volume as an independent realization of a stochastic ergodic process associated to the exceedance probability function $P(t-t_i|t_i)$.

The groundwater storage $S(t)$ contained in the control volume is given by the sum of all transport volumes infiltrating at increasing injection times t_i whose travel times are shorter than $t-t_i$, which reads as

$$S(t)=\int_{-\infty}^{t} I(t_i)P(t-t_i|t_i)dt_i. \tag{1}$$

The time rate variation of water storage may be obtained by differentiating equation (1) with respect to t. Using the Leibniz rule, it follows that

$$\frac{dS}{dt}=I(t)-\int_{-\infty}^{t} I(t_i)p(t-t_i|t_i)dt_i \tag{2}$$

where $p(t-t_i|t_i)(s^{-1})$ is the probability density function obtained by differentiating $P(t-t_i|t_i)$ with respect to t. equation (2) can be seen as a mass balance equation for the control volume where the right-hand side is the algebraic sum of all incoming and outgoing fluxes. Consequently, one can write

$$Q(t)+E(t)=\int_{-\infty}^{t} I(t_i)p(t-t_i|t_i)dt_i. \tag{3}$$

To evaluate the individual contributions of $Q(t)$ and $E(t)$ in equation (3), one should distinguish between the transport volumes that will be drained by subsurface flow and the ones that will be uptaken by evapotranspiration processes. As shown in Figure 1b, the travel time can be a travel time to subsurface flow t_Q or a travel time to evapotranspiration t_E. Defining $\theta(t_i) \in [0, 1]$ as the infiltration partition function that expresses the relative fraction of transport volumes, injected at t_i, that will leave the subcatchment as subsurface flow [see e.g., *Bertuzzo et al.*, 2013 for more details], $p(t-t_i|t_i)$ can now be written as

$$p(t-t_i|t_i)=\theta(t_i)p_Q(t-t_i|t_i)+[1-\theta(t_i)]p_E(t-t_i|t_i). \tag{4}$$

Finally, one may write the individual contributions in equation (3) as

$$Q(t)=\int_{-\infty}^{t} I(t_i)\theta(t_i)p_Q(t-t_i|t_i)dt_i \tag{5}$$

$$E(t)=\int_{-\infty}^{t} I(t_i)[1-\theta(t_i)]p_E(t-t_i|t_i)dt_i. \tag{6}$$

To derive an analytical solution for $p_Q(t-t_i|t_i)$ and $p_E(t-t_i|t_i)$, one shall write the mass conservation of the generic transport volume. Let $I(t_i)dt_iP(t-t_i|t_i)$ be the fraction of the transport volume injected at time t_i that is still inside the subcatchment at time t. Assuming that part of the transport volume is uptaken by Q and E at time t following a random sampling process, the sought mass conservation equation reads

$$\frac{d[I(t_i)dt_iP(t-t_i|t_i)]}{dt}=-[Q(t)+E(t)]\frac{I(t_i)dt_iP(t-t_i|t_i)}{S(t)}. \tag{7}$$

Equation (7) states that Q and E drive the rate of change of the transport volume proportionally to its relative abundance within the water storage—according to the random sampling assumption—given by the ratio of the transport volume over the total storage at the right-hand side. Equation (7) leads to the first-order, homogeneous, linear ODE with nonconstant coefficients

$$\frac{dP(t-t_i|t_i)}{dt}+\frac{Q(t)+E(t)}{S(t)}P(t-t_i|t_i)=0, \tag{8}$$

whose solution, after imposing the initial condition $P(0|t_i)=1$, reads as

$$P(t-t_i|t_i)=e^{-\int_{t_i}^{t}\frac{Q(x)+E(x)}{S(x)}dx}. \tag{9}$$

By replacing equation (4) into equation (8) and using the result from equation (9), one finally obtains

$$p_Q(t-t_i|t_i)=\frac{Q(t)}{S(t)\theta(t_i)}e^{-\int_{t_i}^{t}\frac{Q(x)+E(x)}{S(x)}dx} \tag{10}$$

$$p_E(t-t_i|t_i)=\frac{E(t)}{S(t)[1-\theta(t_i)]}e^{-\int_{t_i}^{t}\frac{Q(x)+E(x)}{S(x)}dx}. \tag{11}$$

Equations (10) and (11) express the travel time distributions of transport volumes infiltrating at time t_i that leave the domain through subsurface and evapotranspiration.

2.2. Energy Transport

To derive the travel time formulation of energy transport, we consider temperature as a passive-reactive scalar carried by water, as *Bertuzzo et al.* [2013] also assumed for chemical tracers. On one side, passivity implies that water temperature does not affect the advection field. On the other side, reactivity implies that the amount of thermal energy of a generic transport volume is not conserved during the transport processes.

Let $T(t-t_i,t_i)(\mathrm{K})$ be the temperature at time t of the transport volume injected at time t_i. The assumption that $T(t-t_i,t_i)$ does not depend on any spatial variable can be reasonably accepted if the spatial correlation scale of the infiltration field is much larger than the one of the heterogeneous reactive and advective processes. Similar considerations have been used to derive other travel time formulations of transport for passive-reactive scalars [e.g., *Benettin et al.*, 2013b]. Point sources are instead a delicate subject, as they tend to provide inherently stochastic processes [*Dagan et al.*, 1990; *Rinaldo et al.*, 1989]. One may express the internal energy of the groudwater storage $H(t)$ (Jm^{-2}) at time t as

$$H(t)=\rho c_p\int_{-\infty}^{t} I(t_i)T(t-t_i,t_i)P(t-t_i|t_i)dt_i, \tag{12}$$

where ρ (kgm^{-3}) and c_p $(\mathrm{Jkg}^{-1}\mathrm{K}^{-1})$ are density and specific heat of water. By differentiating equation (12) using the Leibniz rule, one my express the time rate variation of the energy of the water storage as

$$\frac{dH}{dt}=\rho c_p I(t)T_I(t)-\rho c_p\int_{-\infty}^{t} I(t_i)T(t-t_i,t_i)p(t-t_i|t_i)dt_i+\rho c_p\int_{-\infty}^{t} I(t_i)P(t-t_i|t_i)\frac{dT(t-t_i,t_i)}{dt}dt_i. \quad (13)$$

Equation (13) is the energy balance equation for the control volume and the right-hand side is the algebraic sum of the incoming and outgoing energy fluxes. In particular, the first term is the energy gained from infiltration $\phi_I(t)$ (Wm^{-2}), where $T_I(t)(\mathrm{K})$ is the temperature of the water volume infiltrating at time t. The second terms represents the advective energy fluxes driven by subsurface flow $\phi_Q(t)$ and evapotranspiration $\phi_E(t)$

$$\phi_Q(t)+\phi_E(t)=-\rho c_p\int_{-\infty}^{t} I(t_i)T(t-t_i,t_i)p(t-t_i|t_i)dt_i. \quad (14)$$

The third term includes all the reactive energy processes $\phi_\Delta(t)$ affecting the time evolution of water temperature

$$\phi_\Delta(t)=\rho c_p\int_{-\infty}^{t} I(t_i)P(t-t_i|t_i)\frac{dT(t-t_i,t_i)}{dt}dt_i. \quad (15)$$

An analytical solution for $T(t-t_i,t_i)$ can be obtained by writing the energy conservation of the transport volume. Let $\rho c_p I(t_i)dt_i T(t-t_i,t_i)P(t-t_i|t_i)[\mathrm{Jm}^{-2}]$ be the energy of the transport volume fraction that is still inside the subcatchment at time t. Recalling that $Q(t)$ and $E(t)$ follow a random sampling process among all transport volumes, the energy conservation equation reads as

$$\begin{aligned}\rho c_p\frac{d[I(t_i)dt_iP(t-t_i|t_i)T(t-t_i,t_i)]}{dt}=&-\rho c_p\left[Q(t)+E(t)\right]\frac{I(t_i)dt_iP(t-t_i|t_i)}{S(t)}T(t-t_i,t_i)\\&+\rho c_pI(t_i)dt_iP(t-t_i|t_i)\frac{[T_s(t)-T(t-t_i,t_i)]}{K_s}.\end{aligned} \quad (16)$$

The first term at the right-hand side of equation (16) represents the advection-driven energy loss due to $Q(t)$ and $E(t)$, which is proportional to the relative abundance of the transport volume in the water storage, according to the random sampling assumption. The second term represents the energy variation due to the reactive processes. A simple yet reasonable parametrization for this term has been introduced by forcing the water-soil thermal exchange to incorporate the effect of all the underlying reactive processes. In this case, soil temperature $T_s(t)$ should act as an external forcing that follows the daily and seasonal cycles resulting from the surface energy budget, which depends on land use, presence of snow/ice cover and slope exposure. Accordingly, the water-soil thermal exchange is modeled as a one way-coupled system and the transport volume experiences an energy gain/loss proportional to the difference between soil temperature and water temperature. Recalling that the spatial correlation of infiltration is assumed much larger than the one of reactive processes, we can consider the amount of energy exchanged between water and soil as a function of the contact time, disregarding the specific trajectory followed by the transport volume. K_s (s) is an effective parameter influencing the characteristic time of the water-soil thermal exchange.

Recalling equation (7), after proper simplifications equation (16) leads to the following first-order, nonhomogeneous, linear ODE with nonconstant coefficients

$$\frac{dT(t-t_i,t_i)}{dt}+\frac{T(t-t_i,t_i)}{K_s}=\frac{T_s(t)}{K_s}. \quad (17)$$

The analytical solution of equation (17), sought by imposing the initial condition $T(0,t_i)=T_I(t_i)$, reads

$$T(t-t_i,t_i)=\left[T_I(t_i)+\int_{t_i}^{t}\frac{T_s(x)}{K_s}e^{(x-t_i)/K_s}dx\right]\cdot e^{-(t-t_i)/K_s}. \quad (18)$$

One may notice that, with respect to equation (9), there is an additional term that sums up to the initial condition, arising from the nonhomogeneous nature of the ODE. Two sample solutions of equation (18), obtained for two different values of K_s, are shown in Figure 2. Equation (18) reduces to the much simpler form of equation (19) when assuming a constant soil temperature.

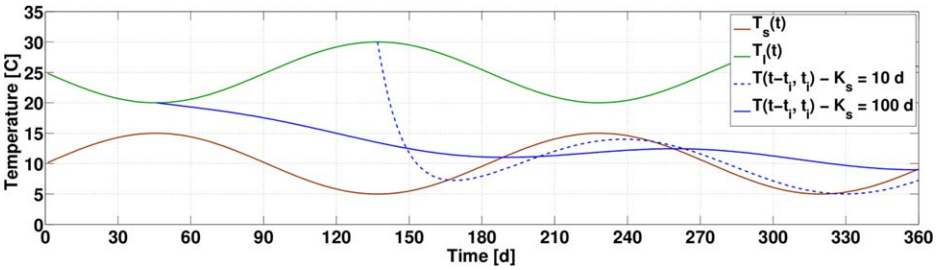

Figure 2. Sample solutions of equation (18) for two different values of K_s. The solutions are obtained considering a constant storage $S(t) = 5$ m and the shown sinusoidal evolutions for $T_s(t)$ and $T_l(t)$.

$$T(t-t_i, t_i) = T_l(t_i)e^{-(t-t_i)/K_s} + T_s\left[1-e^{-(t-t_i)/K_s}\right]. \tag{19}$$

Recalling equations (8), (12), and (17), equations (14) and (15) finally read

$$\phi_Q(t) + \phi_E(t) = \frac{Q(t)+E(t)}{S(t)}H(t) \tag{20}$$

$$\phi_\Delta(t) = \frac{\left[\rho c_p S(t)T_s(t) - H(t)\right]}{K_s}. \tag{21}$$

The following section will show how the energy balance equation (13) can be efficiently solved using equations (20) and (21) to express the energy fluxes in terms of the state variables $S(t)$ and $H(t)$.

Special attention has to be paid when applying the proposed framework to Alpine catchments, where the passivity assumption may break down. In fact, when water temperature approaches 0°C, the freezing process affects mass transport dynamics. The relaxation of the passivity assumption would require an additional temperature-dependent term in the mass balance equation (7) to account for the probability that the transport volume undergoes freezing and melting processes. Moreover, the energy balance equation (16) should also be extended to account for the latent heat fluxes associated to freezing and melting. Although a fully coupled description of mass and energy transport in an active-scalar travel time framework seems feasible, it would certainly require additional and not desirable parametrizations. In the following section, we therefore propose a different solution for reliable applications of the passive-scalar based model to Alpine catchments, based on the physical description of surface processes provided by Alpine3D.

3. Implementation for Alpine Catchments

This section presents the implementation for Alpine catchments of the spatially explicit hydrothermal response model. To properly account for soil water freezing, we implement the derived equations in the physical model Alpine3D, which simulates local scale snow processes and transport dynamics in the surface soil layer. The thickness of this layer is chosen so that the seasonal temperature variations at the bottom do not induce water freezing. In fact, the field investigations carried out by *Jaesche et al*. [2003] and *Bayard et al*. [2005] in high Alpine catchments have shown that temperature does not drop below the freezing point at depth larger than few meters. Accordingly, the assumptions of the travel time formulation hold for the simulation of the transport dynamics at subcatchment scale using the boundary conditions provided by Alpine3D in terms of mass and energy fluxes at the bottom of the surface soil layer.

For a better description of the underlying hydrological processes, the travel time model accounts for two control volumes below the surface soil layer solved by Alpine3D, namely a upper and a lower compartment, as shown in Figure 3. A similar model setup was also adopted e.g., by *Benettin et al*. [2013b] and *Bertuzzo et al*. [2013]. In fact, the general solution presented in section 2 can be applied to each control volume provided that the corresponding incoming and outgoing water and energy fluxes are considered.

3.1. Streamflow Simulation

The flow simulation at subcatchment scale is carried out considering that the portion $I'(t) = \min\{R_{max}, I(t)\}$ of the infiltrating water $I(t)$ (m s^{-1}) at the bottom of the surface layer, given as boundary condition by

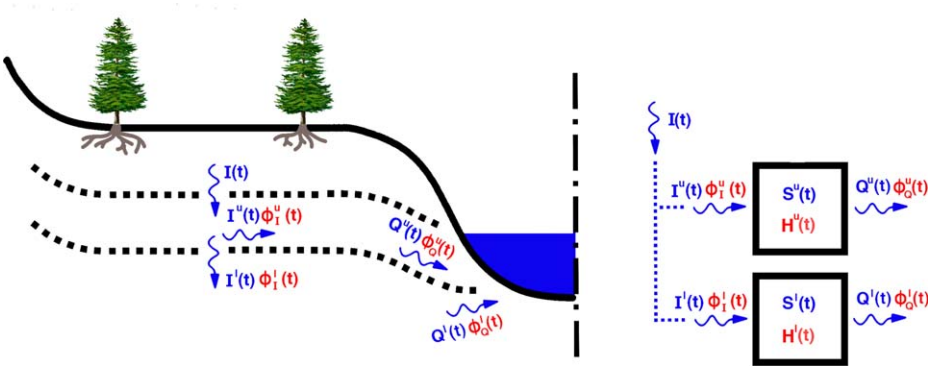

Figure 3. Schematic representation of the mass and energy fluxes associated to the two modeled soil compartments. The upper compartment has a groundwater storage $S^u(t)$ with energy $H^u(t)$, while the lower one has a groundwater storage $S^l(t)$ with energy $H^l(t)$ (for an explanation of the variables see section 3.).

Alpine3D, drains directly into the lower compartment, where R_{max} (m s^{-1}) is the maximum recharge rate. The exceeding part $I^u(t)=I(t)-I^l(t)$ feeds the upper compartment. We assume that the control volumes are not affected by evapotranspiration fluxes, which take place in the surface soil layer and are fully simulated by Alpine3D. Accordingly, we assign $E^u(t)=E^l(t)=0$. The subsurface flows from the upper and lower compartments, $Q^u(t)$ and $Q^l(t)$ (m s^{-1}) respectively, are collected by the stream and transported to the subcatchment outlet. Therefore, the hydrologic response at subcatchment scale can be described by two mass balances in the soil compartments (equations (22) and (23), which are analogous to equation (2)) and a mass balance in the stream (equation (24)).

$$\frac{dS^u(t)}{dt}=I(t)-\min\{R_{max},I(t)\}-Q^u(t) \tag{22}$$

$$\frac{dS^l(t)}{dt}=\min\{R_{max},I(t)\}-Q^l(t) \tag{23}$$

$$Q^{out}(t)=Q^{in}(t)+[Q^u(t)]+Q^l(t)]A \tag{24}$$

where $S^u(t), S^l(t)$ (m) are the water storages in the upper and lower compartment. $Q^{in}(t), Q^{out}(t)$ $(\mathrm{m^3 s^{-1}})$ are the streamflows at the inlet and outlet of the stream and A $(\mathrm{m^2})$ is the area of the subcatchment. Equation (24) embeds the assumption of instantaneous advection in the stream, which can be reasonably accepted considering that open channel flow is orders of magnitude faster than water transport in the soil compartments.

In the most general travel time framework, $Q^u(t)$ and $Q^l(t)$ are expressed by equation (5). Here we assume that the hydrologic response of the control volumes is linear and time-invariant, as the water age mixing induced by soil moisture dynamics mainly occurs in the surface soil layer, simulated by Alpine3D. Similar assumptions were introduced also by *Botter et al.* [2010]. Consequently, $Q^u(t)$ and $Q^l(t)$ can be expressed by the convolution integrals

$$Q^u(t)=\int_{-\infty}^{t} I^u(t_i)p^u(t-t_i)dt_i \tag{25}$$

$$Q^l(t)=\int_{-\infty}^{t} I^l(t_i)p^l(t-t_i)dt_i \tag{26}$$

where $p^u(t-t_i)$ and $p^l(t-t_i)(\mathrm{s^{-1}})$ are the unconditional travel time distributions in the two soil compartments, obtained as special cases of equation (10) under the stationarity assumption. Here we adopt exponential distributions, whose mean values τ^u and τ^l are the average travel times in the two soil compartments. It can be easily shown that, in this case, the expressions resulting from equations (25) and (26) are equivalent to the solution of linear reservoirs, i.e., $Q^u(t)=S^u(t)/\tau^u$ and $Q^l(t)=S^l(t)/\tau^l$. Previous investigations [e.g., *Alexander*, 1972; *Pilgrim et al.*, 1982] suggested that the average travel time can be expressed as a power law of the subcatchment size, i.e., $\tau^u=\bar{\tau}^u(A/A_{tot})^{1/3}$ and $\tau^l=\bar{\tau}^l(A/A_{tot})^{1/3}$, where A_{tot} $(\mathrm{m^2})$ is the area of the entire

catchment. Assuming such a scaling, the coefficients $\bar{\tau}^u, \bar{\tau}^l$ (s) can be assumed valid for all subcatchments and obtained through calibration [*Schaefli et al.*, 2014].

The algorithm is structured in such a way that equations (22), (23), and (24) are initially solved for headwater subcatchments. In the following steps, the outgoing flows $Q^{out}(t)$ from streams of order 1 are summed up to provide the incoming streamflow $Q^{in}(t)$ for the streams of higher order. The scheme proceeds until $Q^{in}(t)$ and $Q^{out}(t)$ are calculated for each node of the stream network. The values at points along the streams between the network nodes are obtained through linear interpolation.

3.2. Stream Temperature Simulation

Temperature simulation at subcatchment scale is based on the solution of a system similar to equations (22), (23), and (24). Here, two equations describe the energy balance in the soil compartments (equations (27) and (28), which are analogous to equation (13)) and one equation describes the energy balance in the stream (equation (29)).

$$\frac{dH^u(t)}{dt} = \phi_I^u(t) - \phi_Q^u(t) + \phi_\Delta^u(t) \tag{27}$$

$$\frac{dH^l(t)}{dt} = \phi_I^l(t) - \phi_Q^l(t) + \phi_\Delta^l(t) \tag{28}$$

$$\phi_Q^{out}(t) = \phi_Q^{in}(t) + [\phi_Q^u(t) + \phi_Q^l(t)]A + \sum \phi^{na} \tag{29}$$

$H^u(t)$ and $H^l(t)(\mathrm{Jm}^{-2})$ are the energy of the groundwater storages in the upper and lower soil compartments. $\phi_I^u(t) = \rho c_p I^u(t) T_I(t)$ and $\phi_I^l(t) = \rho c_p I^l(t) T_I(t)(\mathrm{Wm}^{-2})$ are the incoming energy fluxes in the two soil compartments and are functions of the temperature of infiltrating water $T_I(t)$. The infiltrating water is assumed to be in local thermal equilibrium with the bottom of the surface layer, whose temperature $T_s(t)$ is given as boundary condition by Alpine3D.

The outgoing energy fluxes can be expressed, recalling equation (20), as $\phi_Q^u(t) = Q^u(t) H^u(t)/S^u(t)$ and $\phi_Q^l(t) = Q^l(t) H^l(t)/S^l(t)$. One may notice that, owing the absence of evapotranspiration fluxes below the surface soil layer, we can assign $\phi_E^u(t) = \phi_E^l(t) = 0$. According to equation (21), the water-soil thermal exchange fluxes are $\phi_\Delta^u(t) = [\rho c_p S^u(t) T_s(t) - H^u(t)]/K_s$ and $\phi_\Delta^l(t) = [\rho c_p S^l(t) \overline{T_s} - H^l(t)]/K_s$. In the upper compartment, we assume the soil temperature to be equal to $T_s(t)$ and, in the lower compartment, to be constant and equal to the time average $\overline{T_s}$ (similar considerations were also used in, e.g., *Peters-Lidard et al.* [1997]).

Equation (29) refers to the energy balance in the stream. $\phi_Q^{in}(t) = \rho c_p Q^{in}(t) T_Q^{in}(t)$ and $\phi_Q^{out}(t) = \rho c_p Q^{out}(t) T_Q^{out}(t)$ (W) are the advective energy fluxes at the inlet and at the outlet of the stream. $T_Q^{in}(t)$ and $T_Q^{out}(t)$ are the temperatures of the incoming and outgoing streamflow. $\sum \phi^{na}$ is the sum of the nonadvective energy fluxes, taking place both at the water surface–sensible heat flux $\phi_h(t)$, latent heat flux $\phi_e(t)$, and net radiative flux $\phi_r(t)$–and at the river bed–conductive heat flux $\phi_g(t)$ and friction dissipation $\phi_f(t)$. These fluxes are not accounted for in the proposed travel time framework, which only describes advective fluxes, but standard formulations can be found in literature [e.g., *Brown*, 1969].

$$\phi_h(t) = \rho_a c_{pa} C_h U_a [T_a(t) - T_c(t)] w l \tag{30}$$

$$\phi_e(t) = (\rho_a 0.622 L/P_a) C_e U_a [e_a(t) - e_c(t)] w l \tag{31}$$

$$\phi_r(t) = \left[(1-\alpha) R_s(t) + R_l(t) - \epsilon \sigma T_c(t)^4\right] w l \tag{32}$$

$$\phi_g(t) = K_g \frac{T_s(t) - T_c(t)}{\Delta z} w l \tag{33}$$

$$\phi_f(t) = \gamma \frac{Q^{in}(t) + Q^{out}(t)}{2} \Delta h, \tag{34}$$

where U_a (m s^{-1}) is the wind velocity, T_a (K) is the air temperature, $e_a(t)$ (Pa) is the atmospheric vapour pressure, R_s and R_l (W m^{-2}) are incoming short-wave and long-wave radiations. C_h and C_e (-) are the bulk coefficients for sensible and latent heat, which are assumed to be equal. Alpine3D provides a fully distributed

Table 1. A Priori Parameter Ranges Used for Uniform Parameter Sampling During Monte Carlo Simulations and Sample Set Providing the Best Match With Measured Streamflow and Temperature[a]

Parameter	Lower Limit	Upper Limit	Best Performance
R_{max} (mm/d)	5.0	50.0	12.2
$\bar{\tau}^u$ (d)	1.0	100.0	67.7
$\bar{\tau}^l$ (d)	100.0	600.0	288.0
K_s (d)	10.0	500.0	24.7

[a]Stream temperature simulation is affected by all the listed parameters, while stream flow is affected only by the first three.

and physical description of all these variables [*Lehning et al.*, 2002; *Stössel et al.*, 2010], so that no parametrization is necessary for the simulation of the nonadvective energy fluxes.

ρ_a ($\mathrm{kgm^{-3}}$), c_{pa} ($\mathrm{Jkg^{-1}K^{-1}}$), and P_a (Pa) are density, specific heat, and total atmospheric pressure, respectively. $T_c \simeq (T_Q^{in}+T_Q^{out})/2$ (K) is the stream temperature. $e_c(t)$ (Pa) is the saturation vapor pressure at the stream surface. α (-) is the water albedo, ϵ (-) is the emissivity of water, σ ($\mathrm{Wm^{-2}K^{-4}}$) is the Stefan-Boltzmann constant, K_g ($\mathrm{Wm^{-1}K^{-1}}$) is the soil thermal conductivity, and Δz (m) is the depth of the surface layer of soil solved by Alpine3D. γ ($\mathrm{Nm^{-3}}$) is the specific weight of water and Δh (m) is the altitude difference between stream inlet and outlet. l and w (m) are length and width of the stream, the former retrieved from the geomorphological analysis of the digital terrain model and the latter calculated with the relation $w(t)=12.0\left\{[Q^{in}(t)+Q^{out}(t)]/2\right\}^{0.49}$, proposed by *Magnusson et al.* [2012].

Once the mass fluxes in the soil compartments are calculated, equations (27), (28), and (29) can be solved for each subcatchment to calculate water temperature $T_Q^{out}(t)$ at the outlet of the stream. Similarly to the case of streamflow modeling, the system is initially solved for headwater subcatchments. In the following steps, outgoing energy fluxes $\phi_Q^{out}(t)$ from streams of order 1 are summed up to provide the incoming energy flux $\phi_Q^{in}(t)$ to streams of higher order. The scheme proceeds until $\phi_Q^{in}(t)$ and $\phi_Q^{out}(t)$ are calculated for each node of the stream network. The values at points along the streams are obtained through linear interpolation. The coupled hydrothermal response model has four parameters to calibrate, summarized in Table 1.

4. Case Study and Simulation Setup

The Dischma valley is located in the eastern part of the Swiss Alps, as shown in the inset of Figure 4. The catchment, closed at Dischma Kriegsmatte, drains an area of 43.3 $\mathrm{km^2}$ and has an elevation range from 1677 to 3130 m. The land use is 36% subalpine meadow, 34% rock, and the remaining part mainly forest and bushes [*Swiss Federal Office for Statistic*, 2001]. Glaciers cover only 2% of the catchment.

Since part of the model simulates mass and energy dynamics within the river network, the Taudem routines [*Tarboton*, 1997] are used to extract the stream network and the subcatchment distribution based on the information provided by digital elevation maps. The geomorphological analysis of the catchment, applied

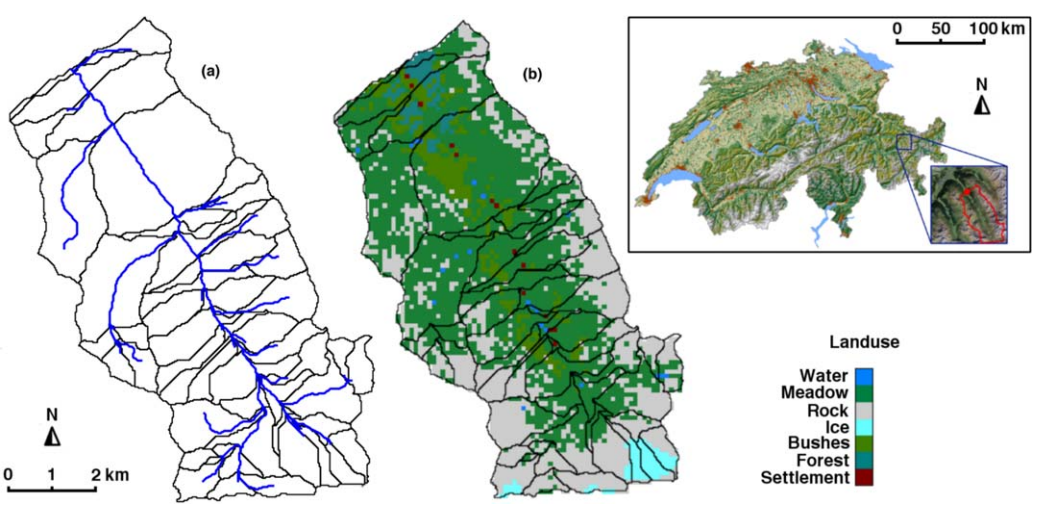

Figure 4. (a) Subcatchments and stream network delineation obtained applying the Taudem routines on a 25 m resolution digital elevation map [*SwissTopo*, 2005] and (b) 100 m resolution land use map of the Dischma catchment [*Swiss Federal Office for Statistic*, 2001].

to a 25 m resolution digital elevation map, delineated 55 subcatchments, as shown in Figure 4a. This relatively high number of subcatchments is adopted to validate the assumption of having source areas much smaller than the correlation scale of reactive and advective processes, as stated in section 2. A 100 m resolution land use map of the catchment is shown in Figure 4b.

Alpine3D simulations are carried for the period 1 October 2011 to 1 October 2012, which is used for the calibration of the hydrothermal model, and 1 October 2012 to 1 October 2013, which is instead used for the model validation. We picked the starting date of the simulation periods in order to have a snow-free initial condition.

The Alpine3D simulations are based on the hourly records of 18 high Alpine automatic weather and snow stations (IMIS), deployed in the area by the Swiss Federal Institute for Snow and Avalanche Research (SLF) in cooperation with the Swiss mountain cantons. Measured parameters include wind, air temperature, relative humidity, snow depth, surface temperature, soil temperature, reflected short-wave radiation, and three temperatures within the snow cover. More detailed information can be found in *Lehning et al*. [1999].

The rectangular domain covers an area of 12.8 km $\times$ 15.4 km containing the Dischma catchment and is meshed with squared elements of 100 m side length. The temporal resolution is 1 h. The main source of error affecting Alpine3D simulations lies in the average distance between the meteo-stations, which may not be sufficient to perform an interpolation able to capture the small-scale variability of the atmospheric fields. Therefore, Alpine3D generally tends to overestimate snow deposition on steep terrains at high altitudes that, in addition, are smoothed according to spatial resolution of the digital elevation map. Such interpolation errors may ultimately result in an wrong estimation of the streamflow volume at the catchment outlet.

The Alpine3D simulations show that, at a depth of 5 m, soil temperature variations do not induce water freezing at any time of the year. We therefore use the local-scale description of infiltration and soil temperature evolution at this depth as boundary conditions to apply the model described in section 3 for the hydrothermal response simulation of the catchment.

No information is available to assign a priori the initial conditions $S^u(0), S^l(0)$ and $H^u(0), H^l(0)$. Imprecise initial conditions result in a mismatch between modeled and measured values at the onset of the simulation, but their influence is lost after few months. Therefore, we perform an additional hydrothermal simulation for the period 1 October 2010 to 1 October 2011, imposing arbitrary initial conditions, and use the values of S^u, S^l, and H^u, H^l at the end of this simulation as initial conditions for the calibration period.

5. Results and Discussion

5.1. Sensitivity, Calibration, and Validation

Given that the model parameters are not representative of the local-scale processes but of the global behavior of the subcatchment system, model calibration is in general a necessary operation. However, reasonable parameter ranges can be assigned owing to their direct physical meaning. 10^4 Monte Carlo simulations are initially carried out to fully explore the parameter space shown in Table 1 and to investigate the model sensitivity.

The fixed parameters are water albedo α=0.1, water density $\rho = 1000$ $(\mathrm{kg\,m^{-3}})$, air density ρ_a=1.30 $(\mathrm{kg\,m^{-3}})$, atmospheric pressure $P_a = 101325$ (Pa), water heat capacity $c_p = 4190$ $(\mathrm{Jkg^{-1}K^{-1}})$, air heat capacity $c_{pa} = 1010$ $(\mathrm{Jkg^{-1}K^{-1}})$, emissivity ϵ=0.995, Stefan-Boltzman constant σ=$5.67 \cdot 10^{-8}$ $(\mathrm{Wm^{-2}K^{-4}})$, and soil thermal conductivity K_g=0.004$(\mathrm{Wm^{-1}K^{-1}})$.

The performance of each corresponding simulation is evaluated by means of two Nash-Sutcliff indices, NS_Q and NS_T [*Nash and Sutcliffe*, 1970], the former telling the quality of the simulation in terms of flow and the latter in terms of temperature. It is noteworthy that no absolute meaning can be attached to the values of these indices, because they depend on the shape of the reference signal [*Schaefli and Gupta*, 2007].

The black lines in Figures 5a and 5b show the distribution of the two indices in the chosen ranges, respectively, for flow and temperature. To evaluate the robustness of the model, we investigated the parameter distribution of the simulations providing a $NS_Q > 0.91$, which corresponds to the 95% quartile of the NS_Q distribution. A further selection is done by extracting the subset of 100 best temperature simulations,

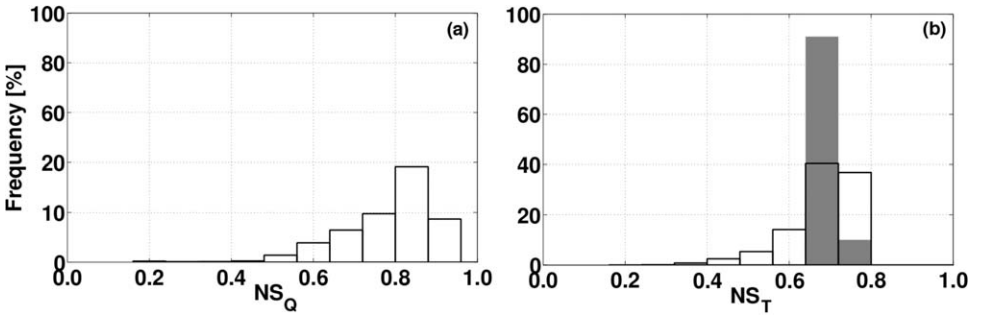

Figure 5. Distribution of the Nash-Sutcliffe indices (a) for streamflow simulations and (b) for stream temperature simulations. Black lines refer to the distributions of all Monte Carlo simulations, the filled bars refer to the distribution of the subset of 100 best temperature simulations ($NS_T > 0.69$) sampled among the 5% best streamflow simulations ($NS_Q > 91$). It is observed that the NS_T distribution of the subset samples among the best temperature simulations of the Monte Carlo sets.

having a $NS_T > 0.69$. In Figure 5b, the filled bars indicate the NS_T distribution in this subset, which is relatively narrow and samples among the largest values of the original set. In Figure 6, the model robustness can be assessed looking at the posterior probability distributions of the parameters, which are located in a well-defined subspace of the prior parameter space. Moreover, it can be noticed that the uncertainty of the hydrological parameters R_{max}, $\bar{\tau}^u$ and $\bar{\tau}^l$ is significantly reduced when streamflow and stream temperature are fitted simultaneously. In fact, the temperature signal contains hydrological information that cannot be directly extrapolated from the streamflow data and therefore helps the understating of the underlying transport processes.

Within the defined subset, the best temperature simulation is characterized by $NS_T = 0.73$ and $NS_Q = 0.92$, obtained with the parameter set listed in Table 1. The good match of the corresponding simulations to the measurements is shown in Figures 7a and 7b, together with the interquartile range of the Monte Carlo simulations. The results suggest that the model is less effective in simulating the transport dynamics in June, when streamflow and temperature are, respectively, underestimated and overestimated. It is worth noting

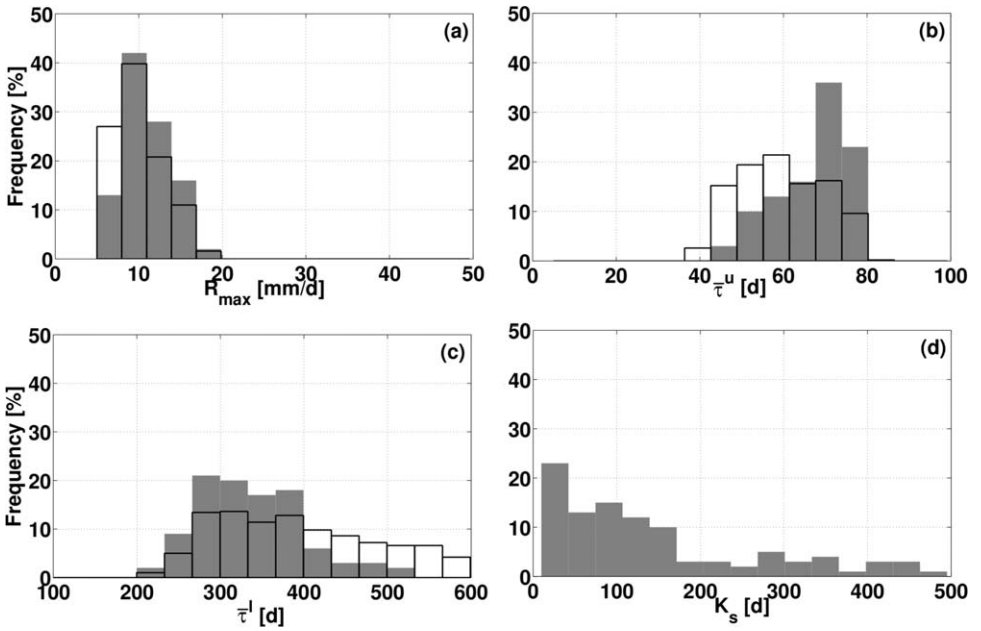

Figure 6. Distribution of the parameters of the hydrothermal model, i.e., (a) R_{max}, (b) $\bar{\tau}^u$, (c) $\bar{\tau}^l$, and (d) K_s. Black lines show the distribution of the best 5% streamflow simulations, i.e., $NS_Q > 0.91$, while filled bars show the distribution of the subset of 100 best temperature simulations, i.e., $NS_Q > 0.91$ and $NS_T > 0.69$. The results suggest that a simultaneous calibration of streamflow and temperature reduces the uncertainty in the estimation of hydrological parameters.

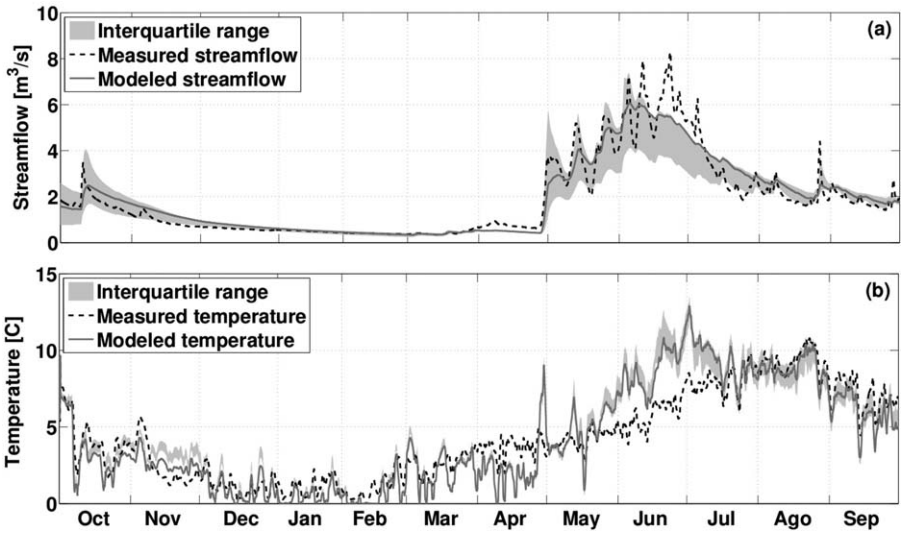

Figure 7. Comparison between measured and modeled (a) streamflow and (b) stream temperature at the outlet, during the calibration period (October 2011 to October 2012). The solid lines represent the modeled results corresponding to the best NS indices (0.92 for streamflow and 0.73 for temperature), the dashed lines represent the measured data. The filled bands correspond to the interquartile range of the Monte Carlo simulations. Signals are averaged over 24 h.

that the adopted *NS*-based calibration for streamflow tends to penalize the correct simulation of the snowmelt peaks in favor of a better representation of the mean flow. However, considering the number and the complexity of involved processes, the general performance turns out to be promising. In particular, we observe good temperature simulations despite of an extremely simple geometric description of the river network and the interactions with the surrounding topography. Moreover, we would like to emphasize that no calibration has been carried out to optimize the boundary conditions provided by Alpine3D, which relies on a physical representation of mass and energy dynamics and is meant to provide reliable predictions at the local scale without prior calibration.

Figures 8a and 8b show the results of the model validation, which is performed by using the best parameters set listed in Table 1. A good match can be observed both for streamflow, with a $NS_Q = 0.83$, and for temperature, with a $NS_T = 0.81$. Such a good agreement suggests that the model setup could be employed for predictive applications, both for hydrological and ecological purposes. The identified range of good

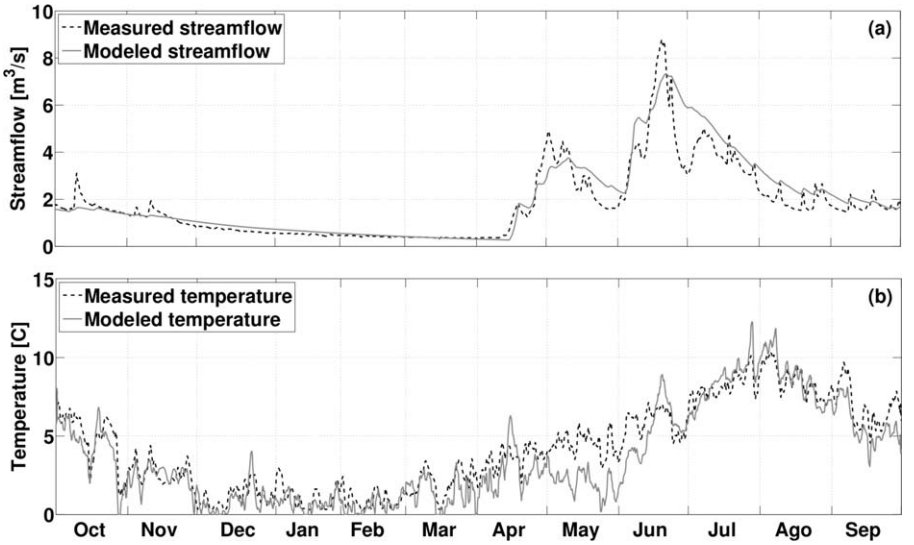

Figure 8. Comparison between measured and modeled (a) streamflow and (b) stream temperature at the outlet during the validation period (October 2012 to October 2013). The corresponding indices are $NS_Q = 0.83$ and $NS_T = 0.81$. Signals are averaged over 24 h.

parameter sets is of course case study specific and their transferability to other environments has to be tested. For additional information on mean travel time estimations for a large variety of Alpine catchments, the reader is referred to *Seeger and Weiler* [2014].

5.2. Temperature Cycles of Subsurface Flow

A numerical experiment is carried out to provide a better insight into the temperature evolution of subsurface flow $T_Q(t)$ at the outlet of the catchment, calculated through the relation $\phi_Q^u(t)+\phi_Q^l(t)=\rho c_p[Q^u(t)+Q^l(t)]T_Q(t)$. This analysis is performed to validate the travel time formulation of the advective energy fluxes. The simulations are carried out with the best parameters set, listed Table 1. The results are shown in Figures 9a and 9b, for the calibration and validation periods, respectively.

We can observe that, in the winter season, the modeled subsurface flow temperature is almost constant and warmer than the stream temperature, which is supported by field investigations of *Leach and Moore* [2014] in Canadian headwater streams. At the onset of the melting season, respectively, in late and mid April for the calibration and the validation periods, we observe a rapid decrease in subsurface flow temperature due the relatively fast transport of cold water in the upper soil layer. Following, we observe an increase of subsurface flow temperature due to an efficient thermal exchange with the warmer soil. The peak of subsurface flow temperature is observed in both cases around the end of June, before the peak of stream temperature occurs. Finally, starting from the end of July, subsurface flow temperature is colder than stream temperature, as also suggested by the field investigations of *Story et al.* [2003] in Canadian headwater streams.

Even though we could not extrapolate relevant information from the available stream temperature data to fully validate these early results, they appear to be consistent with recent studies [e.g., *Kelleher et al.*, 2012; *Luce et al.*, 2014] and with the underlying physical processes. This suggests that the proposed travel time formulation of energy transport may be a useful theoretical basis for thermal regime simulations, even in highly heterogeneous and topographically complex Alpine environments. However, as recently observed by *MacDonald et al.* [2014], there is still a lack of process understanding regarding the relative importance of in-stream energy processes in Alpine catchments. A more in-depth assessment of these model results has therefore to be guided by systematic field-based investigations.

5.3. Hydrologic and Thermal Variability in the Stream Network

This section presents some preliminary results on the spatial distribution of stream flow and temperature. The results focus in particular on the correlation between the hydrothermal patterns and the spatial distribution of hydrometeorological forcings, which might a priori play a determinant role in the hydrologic response of such a small Alpine catchment [*Simoni et al.*, 2011].

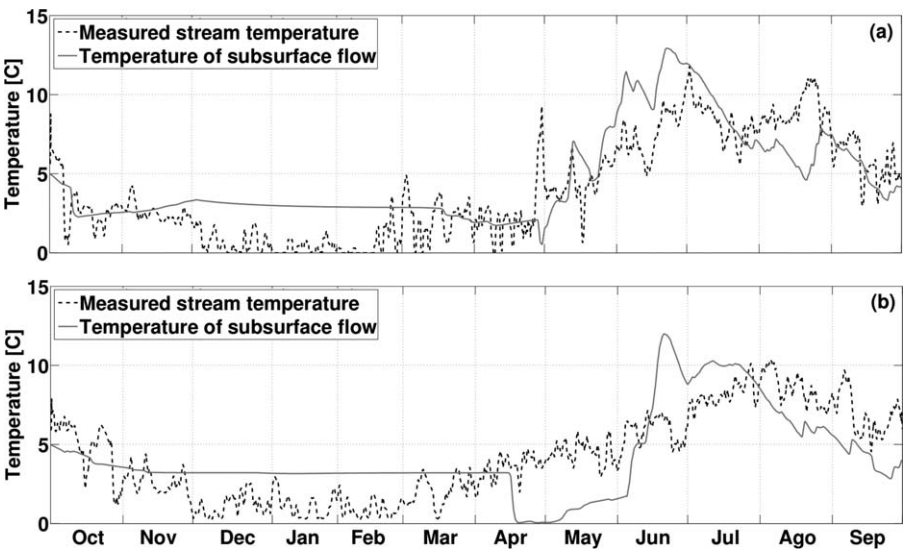

Figure 9. Comparison of the temperature evolution of subsurface flow as opposed to stream temperature at the outlet of the catchment for (a) the calibration period (October 2011 to October 2012) and (b) the validation period (October 2012 to October 2013). Signals are averaged over 24 h.

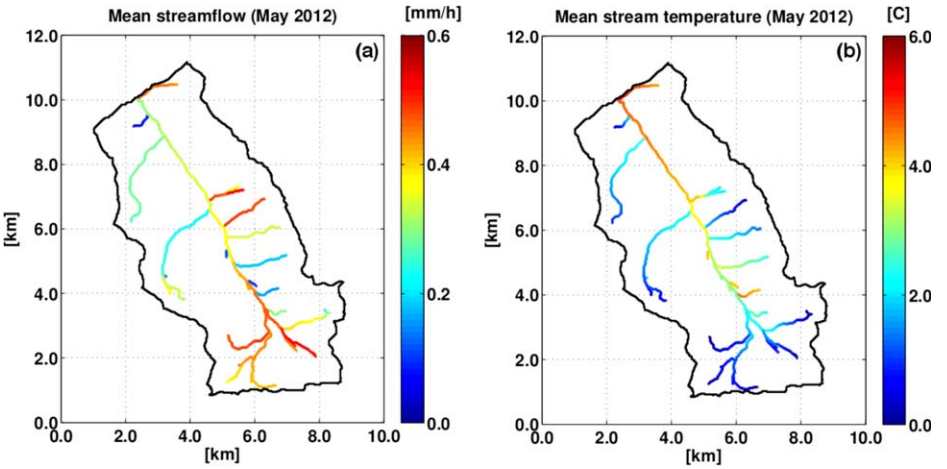

Figure 10. Spatial distribution of (a) specific streamflow (per unit drained area) and (b) stream temperature during the snowmelt event in May 2012. The streamflow pattern strongly reflects the patchy infiltration distribution during snowmelt. The stream temperature pattern reflects the heterogeneous distribution of soil temperature and meteorological forcings.

Figures 10a and 10b show the time-averaged streamflow and temperature over the entire network during May 2012, at the onset of the snowmelt process. The spatial correlation of snow depth is smaller than the size of the catchment [see, e.g., *Trujillo et al.*, 2009], leading to an inhomogeneous distribution of streamflow as also observed by *Smith et al.* [2014] in Alpine environments. Similarly, stream temperature reflects the highly heterogeneous patterns of soil temperature, air temperature, and incoming radiation. These observations support the conclusion that the local-scale description of infiltration and meteorology provided by Alpine3D may add a considerable value to hydrological modeling in Alpine regions.

6. Conclusions

In this paper, we presented a model for distributed simulations of streamflow and stream temperature in Alpine catchments. The model setup relies on the local-scale description of mass end energy fluxes in the surface soil layer, provided by the physical snow model Alpine3D, as boundary conditions for a travel time-based transport model at subcatchment scale. The theoretical derivation of the travel time formulation of water and energy dynamics is based on the water age mixing theory and results in a closed form solution for water temperature evolution in soil compartments.

The model was tested on the Dischma catchment, in the eastern Swiss Alps. The results of a Monte Carlo simulation confirmed that the proposed hydrothermal response model is robust in the tested parameter ranges. Moreover, a simultaneous fitting of streamflow and temperature reduces the uncertainties in hydrological parameters estimations, owing to the additional information on transport processes contained in the temperature data. Given that the temperature is very easy to observe, it would be helpful to calibrate the model only on short times series of stream temperature. However, from a physical perspective, this might be misleading, as a correct hydrological simulation is essential for the description of transported scalar quantities such as chemical solutes or temperature. Future tests will show whether additional snapshot streamflow measurement campaigns are sufficient to well constrain all model parameters.

The calibrated model provides a good fit to the measured streamflow and temperature also in the validation period, which is a promising result considering that no calibration has been carried out to optimize the boundary conditions provided by Alpine3D. The observed ranges of good parameters are case specific and their transferability to other environments has to be tested. However, an effective spatial transferability is also expected, owing to the coupling to Alpine3D and to the explicit accounting for geomorphological complexity. On one side, in fact, a physical and spatially distributed description of snow processes does not require specific calibration and, on the other side, hydrologic residence times are strongly connected to subcatchment size and stream network geometry.

The temporal evolution of subsurface flow, as described by the travel time component of the model, confirms previous experimental observations. In particular, subsurface flow is warmer than streamflow during winter and colder during large part of summer. During the two simulated years, typical observed features are also a drop of subsurface flow temperature at the onset of the melting season, when cold water is transported down to the streams, followed by an increase induced by an efficient thermal exchange with the warming soil. Given the qualitative agreement with field investigations and the support of reasonable physical arguments, we argue that the energy transport in the hydrologic response can be properly cast in a travel time framework using the boundary conditions provided by Alpine3D.

In parallel, we showed that the spatial distribution of streamflow during snowmelt is highly inhomogeneous, owing to the patchy distribution of infiltration. The spatial detail provided by Alpine3D in terms of infiltrating water fluxes is in this sense a noteworthy advantage. Similarly, stream temperature distribution reflects the notable spatial variability of soil temperature, air temperature, and incoming radiation, typical of Alpine regions.

Overall, the travel time formulation extended previous findings to a more complete framework that includes energy transport and lead to an effective description of water soil temperature evolution. Moreover, the proposed coupling with Alpine3D yielded promising results and can present a new avenue for the hydrothermal simulations of Alpine catchments, which has interesting applications, especially in stream ecology.

Notation

$S(t)$ (m)	Groundwater storage per unit area.
$I(t)$ (ms^{-1})	Infiltration.
$Q(t)$ (ms^{-1})	Subsurface flow.
$E(t)$ (ms^{-1})	Evapotranspiration.
t_i (s)	Injection time
$P(t-t_i\|t_i)(\text{-})$	Travel time cumulative distribution function.
$p(t-t_i\|t_i)(\mathrm{s}^{-1})$	Travel time probability density function.
$\theta(t_i)(\text{-})$	infiltration partition function.
$H(t)$ (Jm^{-2})	Energy of the groundwater storage.
$T(t-t_i, t_i)(\mathrm{K})$	Temperature of the transport volume.
$T_I(t)(\mathrm{K})$	Temperature of the infiltrating water.
$\phi(t)(\mathrm{Wm}^{-2})$	Energy flux.
K_s (s)	Characteristic time of thermal exchange.

Acknowledgments
The authors would like to thank the anonymous reviewers for their constructive comments. The research of the second author was supported by a research grant of the Swiss National Science Foundation (SNF, PZ00P2_126607). The streamflow and stream temperature data were obtained from the Swiss Federal Office for the Environment. The meteorological data were obtained from the IMIS (Interkantonales Mess- und Informationssystem) network, MeteoSwiss, and SLF stations. The authors wish to acknowledged Enrico Bertuzzo for his help in the development of the theoretical framework. Mathias Bavay supported the setup of Alpine3D.

References

Alexander, G. (1972), Effect of catchment area on flood magnitude, *J. Hydrol.*, *16*(3), 225–240, doi:10.1016/0022-1694(72)90054-6.
Barnett, T., J. Adam, and D. Lettenmaier (2005), Potential impacts of a warming climate on water availability in snow-dominated regions, *Nature*, *438*(7066), 303–309, doi:10.1038/nature04141.
Bavay, M., M. Lehning, T. Jonas, and H. Löwe (2009), Simulations of future snow cover and discharge in alpine headwater catchments, *Hydrol. Proc.*, *23*(1), 95–108, doi:10.1002/hyp.7195.
Bavay, M., T. Grünewald, and M. Lehning (2013), Response of snow cover and runoff to climate change in high alpine catchments of eastern switzerland, *Adv. Water Resour.*, *55*, 4–16, doi:10.1016/j.advwatres.2012.12.009.
Bayard, D., M. Stähli, A. Parriaux, and H. Flühler (2005), The influence of seasonally frozen soil on the snowmelt runoff at two alpine sites in southern switzerland, *J. Hydrol.*, *309*(1), 66–84, doi:10.1016/j.jhydrol.2004.11.012.
Benettin, P., A. Rinaldo, and G. Botter (2013a), Kinematics of age mixing in advection-dispersion models, *Water Resour. Res.*, *49*, 8539–8551, doi:10.1002/2013WR014708.
Benettin, P., Y. van der Velde, S. van der Zee, A. Rinaldo, and G. Botter (2013b), Chloride circulation in a lowland catchment and the formulation of transport by travel time distributions, *Water Resour. Res.*, *49*, 4619–4632, doi:10.1002/wrcr.20309.
Bertuzzo, E., M. Thomet, G. Botter, and A. Rinaldo (2013), Catchment-scale herbicides transport: Theory and application, *Adv. Water Resour.*, *52*, 232–242, doi:10.1016/j.advwatres.2012.11.007.
Biswal, B., and M. Marani (2010), Geomorphological origin of recession curves, *Geophys. Res. Lett.*, *37*, L24403, doi:10.1029/2010GL045415.
Botter, G., E. Bertuzzo, A. Bellin, and A. Rinaldo (2005), On the lagrangian formulations of reactive solute transport in the hydrologic response, *Water Resour. Res.*, *41*, W04008, doi:10.1029/2004WR003544.
Botter, G., E. Bertuzzo, and A. Rinaldo (2010), Transport in the hydrologic response: Travel time distributions, soil moisture dynamics, and the old water paradox, *Water Resour. Res.*, *46*, W03514, doi:10.1029/2009WR008371.
Brown, G. (1969), Predicting temperatures of small streams, *Water Resour. Res.*, *5*(1), 68–75, doi:10.1029/WR005i001p00068.

Brown, L., and D. Hannah (2007), Alpine stream temperature response to storm events, *J. Hydrometeorol.*, *8*(4), 952–967, doi:10.1175/JHM597.1.
Brown, L., D. Hannah, and A. Milner (2005), Spatial and temporal water column and streambed temperature dynamics within an alpine catchment: Implications for benthic communities, *Hydrol. Proc.*, *19*(8), 1585–1610, doi:10.1002/hyp.5590.
Brutsaert, W. (2005), *Hydrology: An Introduction*, Cambridge Univ. Press, N. Y.
Caissie, D. (2006), The thermal regime of rivers: A review, *Freshwater Biol.*, *51*(8), 1389–1406, doi:10.1111/j.1365-2427.2006.01597.x.
Coutant, C. (1977), Compilation of temperature preference data, *J. Fish. Res. Board Can.*, *34*(5), 720–745, doi:10.1120/f77–115.
Dagan, G. (1990), Transport in heterogeneous porous formations: spatial moments, ergodicity, and effective dispersion. *Water Resour. Res.*, 26, 1281–1290, doi:10.1029/WR026i006p01281.
Finger, D., et al. (2013), Identification of glacial meltwater runoff in a karstic environment and its implication for present and future water availability, *Hydrol. Earth Syst. Sci.*, *17*(8), 3261–3277, doi:10.5194/hess-17–3261-2013.
Hari, R., D. Livingstone, R. Siber, P. Burkhardt-Holm, and H. Guettinger (2006), Consequences of climatic change for water temperature and brown trout populations in alpine rivers and streams, *Global Change Biol.*, *12*(1), 10–26, doi:10.1111/j.1365-2486.2005.001051.x.
Jaesche, P., H. Veit, and B. Huwe (2003), Snow cover and soil moisture controls on solifluction in an area of seasonal frost, eastern alps, *Permafrost Periglacial Process.*, *14*(4), 209–410, doi:10.1002/ppp.471.
Kelleher, C., T. Wagener, M. Gooseff, B. McGlynn, K. McGuire, and L. Marshall (2012), Investigating controls on the thermal sensitivity of Pennsylvania streams, *Hydrol. Process.*, *26*(5), 771–785, doi:10.1002/hyp.8186.
Kurylyk, B., C.-A. Bourque, and K. MacQuarrie (2013), Potential surface temperature and shallow groundwater temperature response to climate change: an example from a small forested catchment in east-central New Brunswick (Canada), *Hydrol. Earth Syst. Sci.*, *17*(7), 2701–2716.
Leach, J. A., and R. Moore (2014), Winter stream temperature in the rain-on-snow zone of the Pacific Northwest: influences of hillslope runoff and transient snow cover, *Hydrol. Earth Syst. Sci.*, *18*, 819–838, doi:10.5194/hess-18-819-2014.
Lehning, M., P. Bartelt, B. Brown, T. Russi, U. Stöckli, and M. Zimmerli (1999), Snowpack model calculations for avalanche warning based upon a new network of weather and snow stations, *Cold Reg. Sci. Technol.*, *30*(1), 145–157, doi:10.1016/S0165-232X(99)00022-1.
Lehning, M., P. Bartelt, B. Brown, and C. Fierz (2002), A physical snowpack model for the swiss avalanche warning: Part iii: Meteorological forcing, thin layer formation and evaluation, *Cold Reg. Sci. Technol.*, *35*(3), 169–184, doi:10.1016/S0165-232X(02)00072-1.
Lehning, M., I. Völksch, D. Gustafsson, T. Nguyen, M. Stähli, and M. Zappa (2006), Alpine3d: A detailed model of mountain surface processes and its application to snow hydrology, *Hydrol. Proc.*, *20*(10), 2111–2128, doi:10.1002/hyp.6204.
Luce, C., B. Staab, M. Kramer, S. Wenger, D. Isaak, and C. McConnel (2014), Sensitivity of Summer Stream Temperatures to Climate Variability in the Pacific Northwest, *Water Resour. Res.*, *50*(4), 3428–3443, doi:10.1002/2013WR014329.
MacDonald, R. J., S. Boon, and J. M. Byrne (2014), A process-based stream temperature modelling approach for mountain regions, *J. Hydrol.*, *511*(0), 920–931, doi:10.1016/j.jhydrol.2014.02.009.
Magnusson, J., T. Jonas, and J. Kirchner (2012), Temperature dynamics of a proglacial stream: Identifying dominant energy balance components and inferring spatially integrated hydraulic geometry, *Water Resour. Res.*, *48*, doi:10.1029/2011WR011378.
Matulla, C., S. Schmutz, A. Melcher, T. Gerersdorfer, and P. Haas (2007), Assessing the impact of a downscaled climate change simulation on the fish fauna in an inner-alpine river, *Int. J. Biometeorol.*, *52*(2), 127–137, doi:10.1007/s00484-007-0107-6.
Mohseni, O., H. Stefan, and J. Eaton (2003), Global warming and potential changes in fish habitat in us streams, *Clim. Change*, *59*(3), 389–409, doi:10.1023/A:1024847723344.
Mutzner, R., E. Bertuzzo, P. Tarolli, S. Weijs, L. Nicotina, S. Ceola, N. Tomasic, I. Rodriguez-Iturbe, M. Parlange, and A. Rinaldo (2013), Geomorphic signatures on brutsaert base flow recession analysis, *Water Resour. Res.*, *49*, 5462–5472, doi:10.1002/wrcr.20417.
Nash, J., and J. Sutcliffe (1970), River flow forecasting through conceptual models part: I. A discussion of principles, *J. Hydrol.*, *10*(3), 282–290, doi:10.1016/0022-1694(70)90255-6.
Peters-Lidard, C., M. Zion, and E. Wood (1997), A soil-vegetation-atmosphere transfer scheme for modeling spatially variable water and energy balance processes, *J. Geophys. Res.*, *102*(D4), 4303–4324, doi:10.1029/96JD02948.
Pilgrim, D., I. Cordery, and B. Baron (1982), Effects of catchment size on runoff relationships, *J. Hydrol.*, *58*(3), 205–221, doi:10.1016/0022-1694(82)90035-X.
Rinaldo, A., and A. Marani (1987), Basin scale model of solute transport, *Water Resour. Res.*, *23*(11), 2107–2118, doi:10.1029/WR023i011p02107.
Rinaldo, A., and I. Rodriguez-Iturbe (1996), Geomorphological theory of the hydrological response, *Hydrol. Proc.*, *10*(6), 803–829, doi:10.1002/(SICI)1099-1085(199606)10:6 <803::AID-HYP373 >3.0.CO;2-N.
Rinaldo, A., A. Marani, and A. Bellin (1989), On mass response functions, *Water Resour. Res.*, *25*(7), 1603–1617, doi:10.1029/WR025i007p01603.
Rinaldo, A., A. Marani, and R. Rigon (1991), Geomorphological dispersion, *Water Resour. Res.*, *27*(4), 513–525, doi:10.1029/90WR02501.
Rinaldo, A., G. Botter, E. Bertuzzo, A. Uccelli, T. Settin, and M. Marani (2006), Transport at basin scales: 1. Theoretical framework, *Hydrol. Earth Syst. Sci.*, *10*(1), 19–29, doi:10.5194/hess-10-19-2006.
Rinaldo, A., K. Beven, E. Bertuzzo, L. Nicotina, J. Davies, A. Fiori, D. Russo, and G. Botter (2011), Catchment travel time distributions and water flow in soils, *Water Resour. Res.*, *47*, W07537, doi:10.1029/2011WR010478.
Schaefli, B., and H. Gupta (2007), Do nash values have value?, *Hydrol. Proc.*, *21*(15), 2075–2080, doi:10.1002/hyp.6825.
Schaefli, B., A. Rinaldo, and G. Botter (2013), Analytic probability distributions for snow-dominated streamflow, *Water Resour. Res.*, *49*, 2701–2713, doi:10.1002/wrcr.20234.
Schaefli, B., L. Nicótina, C. Imfeld, P. Da Ronco, E. Bertuzzo, and A. Rinaldo (2014), Sehr-echo v1. 0: A spatially-explicit hydrologic response model for ecohydrologic applications, *Geosci. Model Dev.*, *7*, 2733–2746, doi:10.5194/gmd-7-2733-2014.
Seeger, S., and M. Weiler (2014), Reevaluation of transit time distributions, mean transit times and their relation to catchment topography, *Hydrol. Earth Syst. Sci.*, *18*(12), 4751–4771, doi:10.5194/hess-18-4751-2014.
Simoni, S., S. Padoan, D. Nadeau, M. Diebold, A. Porporato, G. Barrenetxea, F. Ingelrest, M. Vetterli, and M. Parlange (2011), Hydrologic response of an alpine watershed: Application of a meteorological wireless sensor network to understand streamflow generation, *Water Resour. Res.*, *47*, W10524, doi:10.1029/2011WR010730.
Smith, R. S., R. D. Moore, M. Weiler, and G. Jost (2014), Spatial controls on groundwater response dynamics in a snowmelt-dominated montane catchment, *Hydrol. Earth Syst. Sci.*, *18*(5), 1835–1856, doi:10.5194/hess-18-1835-2014.
Stahl, K., R. Moore, J. Shea, D. Hutchinson, and A. Cannon (2008), Coupled modelling of glacier and streamflow response to future climate scenarios, *Water Resour. Res.*, *44*, W02422, doi:10.1029/2007WR005956.
Stewart, I., D. Cayan, and M. Dettinger (2005), Changes toward earlier streamflow timing across western north America, *J. Clim.*, *18*(8), 1136–1155, doi:10.1175/JCLI3321.1.

Story, A., R. Moore, and J. Macdonald (2003), Stream temperatures in two shaded reaches below cutblocks and logging roads: Downstream cooling linked to subsurface hydrology, *Can. J. For. Res.*, *33*(8), 1383–1206, doi:10.1120/x03-087.

Stössel, F., M. Guala, C. Fierz, C. Manes, and M. Lehning (2010), Micrometeorological and morphological observations of surface hoar dynamics on a mountain snow cover, *Water Resour. Res.*, *46*, W04511, doi:10.1029/2009WR008198.

Swiss Federal Office for Statistic (2001), *Geostat: Version 1997, Swiss Spatial Land Use Statistics Data-Base*, Bern, Switzerland.

SwissTopo (2005), *Dhm25: The Digital Height Model of Switzerland*, Wabern.

Tarboton, D. (1997), A new method for the determination of flow directions and upslope areas in grid digital elevation models, *Water Resour. Res.*, *33*(2), 309–319, doi:10.1029/96WR03137.

Todini, E. (2007), Hydrological catchment modelling: Past, present and future, *Hydrol. Earth Syst. Sci.*, *11*(1), 468–482, doi:10.5194/hess-11-468-2007.

Trujillo, E., J. A. Ramírez, and K. J. Elder, (2009), Scaling properties and spatial organization of snow depth fields in sub-alpine forest and alpine tundra, *Hydrol. Process.*, *23*, 1575–1590, doi:10.1002/hyp.7270.

Trujillo, E., and N. P. Molotch (2014), Snowpack regimes of the Western United States, *Water Resour. Res.*, *50*, 5611–5623, doi:10.1002/2013WR014753.

Ward, J. V., and K. Tockner (2001), Biodiversity: Towards a unifying theme for river ecology, *Freshwater Biol.*, *46*(6), 807–819, doi:10.1046/j.1365-2427.2001.00713.x.